Research Article

Journal of Environmental Nanotechnology

Green-synthesized ZnO-reinforced *Cladophora glomerata*–PVA Biocomposite Films: Physicochemical, Mechanical, Biodegradation and Antibacterial Performance

P. Saraswathi[1], N. Selvam[2*], Umaselvi Muthusamy[3], G. Chandrasekaran[4], R. Vasanthakumar[5] and S. Kalai Selvi[6]

[1]Department of Computer Science and Applications, SRM Institute of Science and Technology, Faculty of Science and Humanities, Vadapalani Campus, Chennai, TN, India
[2]Department of Electrical and Electronics Engineering, M. Kumarasamy College of Engineering, Karur, TN, India
[3]Department of Computer Science and Engineering, P A College of Engineering and Technology, Coimbatore, TN, India
[4]Department of Mechanical Engineering, Lord Jegannath College of Engineering and Technology, Nagercoil, TN, India
[5]Department of Mechanical Engineering, K.S.R. College of Engineering, Tiruchengode, TN, India
[6]Department of Chemistry, Velalar College of Engineering and Technology (Autonomous), Erode, TN, India
Received: 25.07.2026 Accepted: 22.08.2026 Published: xx.xx.xxxx
*selvamaadhu@gmail.com

ABSTRACT

The biocompatible films made from renewable biological materials have received significant interest due to their biodegradable, biocompatible and multifunctional properties. The novelty of this study lies in the dual utilization of *Cladophora glomerata*, with its biomass incorporated into the PVA film matrix and its extract employed as a biological medium for the green synthesis of ZnO nanoparticles. The synthesized ZnO nanoparticles were subsequently incorporated into the biomass–PVA films at 1, 3, and 5 wt.%. In this research, *Cladophora glomerata* was used as a renewable stabilizing agent for ZnO nanoparticles synthesized through a green method and subsequently loaded into biomass–PVA composite films at 1, 3, and 5 wt.%. Successful formation of crystalline hexagonal ZnO was confirmed by XRD, while FTIR indicated the presence of functional groups potentially involved in interactions between biomass, PVA, and ZnO, as evidenced by characteristic peaks at 3410 cm^{-1}, 1636 cm^{-1}, and 1056 cm^{-1}. The synthesized ZnO nanoparticles exhibited an optical absorption edge of 339–341 nm and a zeta potential of −29.29 mV. The DLS-derived hydrodynamic diameter of 339–341 nm likely reflects aggregation in suspension rather than the primary nanoparticle size. Thermal stability was also enhanced when ZnO was added to the neat film, as seen from the DSC analysis, where the main endothermic transition was shifted from 220°C for the neat film to 228°C for the ZnO-incorporated film. The tensile strength decreased from 11.0 ± 0.3 MPa for the biomass–PVA film to 4.5 ± 0.4, 1.5 ± 0.5, and 2.0 ± 0.5 MPa for the 1, 3, and 5 wt.% ZnO films, respectively, likely due to ZnO aggregation, matrix discontinuity, and localized stress concentration, whereas the 1 wt.% ZnO film exhibited the highest elongation at break (90 ± 3%). The liquid uptake for the 5 wt.% ZnO formulation was found to be 125 ± 3%, which reduced from 155 ± 5% in the case of the control film, and all film formulations exhibited more than 70% soil-induced mass loss after seven days. The 3 wt.% ZnO formulation was preferred specifically based on antibacterial performance; however, the most suitable ZnO loading remained application-dependent because the 1 wt.% formulation exhibited the highest elongation at break, whereas the 5 wt.% formulation showed the lowest liquid uptake. The results indicated that the prepared biomass–PVA/ZnO biocomposite can be used as a sustainable and environmentally friendly material in food packaging and biomedical applications.

Keywords: Green synthesis; Colloidal stability; Biodegradability; Endothermic transition; Thermal stability; Biomass.

1. INTRODUCTION

Growing environmental concerns over petroleum-based plastics have increased interest in biodegradable polymer composites derived from renewable resources. Natural polymers reinforced with environmentally friendly nanomaterials offer an attractive alternative because of their biodegradability, biocompatibility, and improved functional performance. Among these materials, poly(vinyl alcohol) (PVA) has gained considerable attention due to its excellent film-forming ability, flexibility, transparency, hydrophilicity, and non-toxicity. However, its poor water resistance, limited mechanical strength, and inadequate antimicrobial activity restrict broader applications. Consequently, the incorporation of natural polymers and inorganic nanoparticles into PVA matrices has emerged as an effective strategy to enhance their mechanical, barrier, and biological properties. Recently, carboxymethyl cellulose (CMC)/PVA hydrogel films

reinforced with honey-mediated green-synthesized ZnO nanoparticles exhibited enhanced tensile strength, antibacterial efficiency exceeding 99%, antioxidant activity above 70%, high cytocompatibility, and approximately 60% biodegradation within 28 days, demonstrating the capability of ZnO nanoparticles to simultaneously improve mechanical, biological, and environmental performance (Mathew *et al.* 2026). Likewise, multifunctional electrospun PVA/chitosan nanofibers containing polydopamine-coated ZnO nanoparticles and black phosphorus nanosheets accelerated diabetic wound healing through sustained Zn^{2+} release, reactive oxygen species scavenging, anti-inflammatory activity, and rapid bacterial inhibition (Li *et al.* 2026).

Green synthesis of metal oxide nanoparticles has become an important strategy for eliminating hazardous chemicals traditionally employed during nanoparticle production. Plant extracts, agricultural wastes, and natural biomolecules have been widely utilized as stabilizing agents for environmentally friendly nanoparticle synthesis (Muralidhar *et al.* 2026). Orange peel-mediated ZnO nanoparticles incorporated into PVA films significantly improved tensile strength, thermal stability, hydrophobicity, and antimicrobial performance for sustainable food-packaging applications (Abhang *et al.* 2025). Similarly, xylan/PVA composite films reinforced with nano-ZnO exhibited improved tensile strength, reduced oxygen and water vapor permeability, enhanced hydrophobicity, and superior thermal stability, demonstrating the effectiveness of ZnO as a multifunctional nanofiller (Yao *et al.* 2025).

Algae have recently emerged as promising renewable resources owing to their rapid growth, abundant polysaccharides, cellulose-rich composition, and naturally occurring bioactive compounds capable of functioning as stabilizing agents. Polysaccharides and other oxygen-containing biological constituents present in algal extracts provide hydroxyl and related functional groups capable of interacting with Zn^{2+} species during precipitation and particle formation. These constituents can assist precursor complexation, nucleation control, and stabilization of the developing ZnO particles. Previous work using *C. glomerata* extract has similarly demonstrated biologically mediated ZnO synthesis and has shown that precursor chemistry affects crystallinity, surface properties, and antimicrobial behavior (Sezen and Aktan, 2025). In addition to nanoparticle synthesis, algal biomass can serve as an environmentally sustainable reinforcement for biodegradable composites. The integrated use of *C. glomerata* is based on two distinct biomass fractions. The extract provides soluble biological constituents that can interact with Zn precursor species during nanoparticle formation, whereas the extraction residue contains a polysaccharide-rich solid fraction that can subsequently interact with the hydroxyl-rich PVA matrix. Thus, a single renewable feedstock is valorized as both a biological synthesis medium and a structural biomass component. For example, algal nanocellulose extracted from *Desmodesmus abundans* was successfully incorporated into PVA bioplastic films, producing biodegradable seed-coating materials with enhanced mechanical properties while significantly improving seed germination and plant growth (Sahu *et al.* 2026). Furthermore, biochemical investigations on *Cladophora glomerata* have demonstrated its rich biochemical composition and sensitivity to environmental stress, indicating its potential as a valuable biomass source for sustainable material development and environmental applications (Çelekli and Alkan, 2024). Existing studies have generally investigated PVA/ZnO films, algal biomass–PVA composites, or biologically synthesized ZnO as separate material strategies. Comparatively less attention has been given to systems in which the same algal feedstock contributes both to ZnO synthesis and to polymer reinforcement. In particular, the combined effects of *Cladophora glomerata*-derived biomass and green-synthesized ZnO on PVA crystallinity, interfacial interactions, thermal behaviour, liquid uptake, mechanical performance, soil-induced mass loss, and antibacterial activity remain insufficiently resolved (Xie *et al*. 2024).

Recent studies demonstrate that ZnO incorporation can modify the mechanical, moisture-related, thermal, and antimicrobial properties of PVA-based biodegradable films. Green-synthesized ZnO/PVA systems have shown improvements in water resistance and antimicrobial performance, while algal biomass has separately been investigated as a renewable reinforcement for PVA matrices. However, differences in biological precursor, nanoparticle loading, matrix composition, and dispersion strongly influence the resulting film properties, making direct comparison and composition-specific evaluation essential (Abdo *et al.* 2024). Biodegradable chitosan/lignin composite films reinforced with banana peel-mediated green-synthesized Ag nanoparticles (AgNPs) were fabricated as sustainable food packaging materials. The AgNPs had an average size of 8.71 ± 2.26 nm, while the optimized CTS-LG5-Ag5 film exhibited >80% antioxidant activity, 99.99% antibacterial efficiency within 3 h, and successfully extended the shelf life of strawberries to 6 days, outperforming commercial packaging (Huynh *et al.* 2026). Aloe vera/xanthan gum hydrogels containing allantoin and salicylic acid also exhibited favorable mechanical properties and swelling behavior for wound-healing applications (Chelu *et al.* 2023). Likewise, active alginate nanocomposite films containing tomato waste-mediated biosynthesized AgNPs were developed for sustainable food packaging. The optimized 3 wt.% AgNP formulation achieved 47.5 MPa tensile strength, reduced water solubility from 68% to 29%, lowered water vapor permeability by 70.9%, and exhibited inhibition zones of 20.2 mm (*S. aureus*) and 18.3 mm (*E. coli*) (Meniche *et al.* 2026).

Boehmite nanoparticle-reinforced CMCS/PVA films further improved mechanical strength, dielectric properties, and thermal stability for flexible electronic applications (Meera and Ramesan, 2023), whereas PBAT composites containing green-derived carbon nanoparticles demonstrated superior mechanical performance, barrier properties, antimicrobial activity, and prolonged food shelf life (Venkatesan *et al.* 2024). Nanotechnology has also expanded into advanced biomedical systems. Electrospun gatifloxacin-loaded polyacrylonitrile (PAN) nanofibers were developed as a sustained ocular drug delivery system for dry eye treatment. The optimized nanofibers exhibited an average diameter of 480 nm, 95% drug entrapment efficiency, 180% swelling index, 90% cumulative drug release over 16 days, and antibacterial inhibition zones of 15 ± 0.31 mm against *E. coli* and 13 ± 0.26 mm against *S. aureus*, resulting in superior corneal healing and tear film stability compared with commercial eye drops (Sahu *et al.* 2023).

Similarly, lignin nanoparticle-reinforced natural rubber nanocomposites exhibited enhanced mechanical properties, UV resistance, antibacterial activity, and biodegradability (Sethulekshmi *et al.* 2024). Chitosan nanoparticles incorporating natural bioactive extracts demonstrated significantly stronger antimicrobial activity than conventional chitosan films against drug-resistant microorganisms (Marei *et al.* 2026). More recently, machine learning-guided nano-QSAR approaches have been successfully integrated with green synthesis strategies to predict low-cytotoxicity nanomaterials prior to synthesis, enabling the development of biocompatibility-requiring graphene quantum dots for sustainable biomedical applications (Ebenezer *et al.* 2026). The optimized 2 mM green-synthesized CeO_2 nanoparticles using Ficus religiosa leaf extract increased the tensile strength from 6.2 MPa to 8.4 MPa, achieved a flexural strength of 18.9 MPa, reduced water absorption to 2.63 ± 0.19%, and slightly improved thermal stability (398–405°C), demonstrating the effectiveness of CeO_2 nanoparticles for sustainable structural composite applications (Jachak *et al.* 2026). Furthermore, comparative investigations involving ZnO nanoparticles synthesized using *Moringa oleifera*, *Terminalia chebula*, and *Aloe vera* extracts demonstrated superior crystallinity, tunable optical properties, and enhanced photocatalytic degradation compared with conventionally synthesized ZnO, confirming the advantages of environmentally friendly synthesis approaches (Kashyap *et al.* 2026).

Previous studies have generally investigated PVA/ZnO composite films, algal biomass-reinforced PVA systems, and biologically synthesized ZnO nanoparticles as separate material-development strategies. In contrast, the present study integrates these approaches through the dual utilization of *Cladophora glomerata*, where the algal extract serves as a biological medium for green ZnO nanoparticle synthesis and the processed residual biomass is subsequently incorporated as reinforcement in the PVA matrix. This integrated biomass-valorization strategy enables more complete utilization of a single renewable feedstock while linking nanoparticle synthesis with composite-film fabrication. The influence of ZnO loading was systematically examined at 0, 1, 3, and 5 wt.% to establish composition-dependent changes in structural organization, interfacial interactions, thermal behavior, liquid uptake, tensile performance, soil-induced mass loss, and antibacterial activity against *Escherichia coli* and *Staphylococcus aureus*. Particular attention was given to the trade-offs generated by ZnO incorporation, since increasing nanoparticle loading can enhance antibacterial performance and reduce liquid uptake while simultaneously influencing matrix continuity, flexibility, and degradation behavior. Rather than defining a universally optimum composition, the formulations were comparatively evaluated to identify application-dependent property balances. Thus, the principal novelty of this work lies in combining algal-assisted ZnO synthesis, residual-biomass reinforcement, controlled nanofiller loading, and multifunctional film evaluation within a single *C. glomerata*/PVA/ZnO system, providing a basis for further development of biodegradable and antibacterial polymer films.

2. MATERIALS AND METHODOLOGY

2.1 Materials

Hydrogen peroxide (H_2O_2), sulfuric acid (H_2SO_4), sodium hydroxide (NaOH), zinc nitrate hexahydrate [$Zn(NO_3)_2{\cdot}6H_2O$], nutrient agar, nutrient broth, ethanol, and poly(vinyl alcohol) were obtained from Star Scientific, Erode, Tamil Nadu, India. Distilled water was employed for reagent preparation and laboratory cleaning.

Crystalline phases of the biomass, ZnO nanoparticles, and composite films were evaluated using a PANalytical Empyrean diffractometer with Cu Kα radiation over a 2θ interval of 20–80° (Acharya *et al.* 2022). Functional groups were identified in transmission mode using a Shimadzu IRSpirit FTIR spectrometer (Husien *et al.* 2026). Surface features and ZnO dispersion were investigated with a Gemini Zeiss scanning electron microscope. Thermal transitions and stability were assessed using a TA Instruments DSC 250 differential scanning calorimeter (Ramesan *et al.* 2024).

2.2 Cultivation and Processing of Algal Biomass

Cladophora glomerata was maintained aseptically in BG11 nutrient solution inside a Binder KBW 240 growth chamber at 25 °C under 5000 lx illumination with alternating 12 h photoperiods. After

cultivation, the algal material was separated using an Eppendorf 5810 R centrifuge and rinsed thoroughly with distilled water. The recovered biomass was dehydrated at 45 °C in a Memmert UF55 forced-air oven and subsequently converted into fine powder using a Retsch GM 200 laboratory mill (Singh *et al.* 2026).

2.3 Preparation of Algal Extract

Powdered *Cladophora glomerata* biomass (10 g) was immersed in 200 mL of 70% ethanol and maintained at ambient temperature for 12 h. Following maceration, the liquid fraction was separated using filter paper and concentrated at 55 °C for 15 min with a Büchi Rotavapor R-100. Part of the concentrated extract was redissolved in 70% ethanol to obtain a 10 mg mL^{-1} stock solution for ZnO nanoparticle preparation and refrigerated at 4 °C. The remaining dried extract was preserved at −20 °C until further testing.

2.4 Purification of Residual Algal Biomass

Following extraction, the dried algal residue was treated with 17.5 wt.% NaOH for 3 h at 100 °C using Heidolph Hei-PLATE Mix 'n' Heat Core reflux assembly. The alkali-treated biomass was rinsed with tap water to neutral pH and air-dried. It was subsequently exposed to 1 M H_2SO_4 under identical operating conditions, followed by thorough washing. Final bleaching was conducted with 5 wt.% H_2O_2 at 100 °C for 3 h under reflux. The purified biomass fraction was then repeatedly rinsed with distilled water and dried before composite preparation. The treatment removed non-polysaccharide impurities; however, possible polysaccharide degradation and structural changes were assessed using XRD, FTIR, and SEM.

2.5 Green Preparation and Analysis of ZnO Nanoparticles

A 100 mL portion of 0.1 M zinc nitrate hexahydrate was combined with 20 mL of *Cladophora glomerata* extract and continuously mixed for 3 h using an IKA C-MAG HS 7 stirrer. The pH was adjusted to 10 by gradually introducing NaOH to promote precipitation (Zhang *et al.* 2023). After pH adjustment, the suspension was aged for 60 min. The precipitate was recovered using a Thermo Scientific Sorvall ST 8 centrifuge at 10,000 rpm for 15 min, washed three times with distilled water, dried at 80 °C for 12 h, and calcined at 400 °C for 2 h under an air atmosphere. Surface structure and elemental composition were assessed using a Gemini Zeiss microscope equipped with EDX. Hydrodynamic diameter and surface charge were measured at 30 °C using a Malvern Zetasizer Pro. Optical absorption between 200 to 800 nm was recorded with a Thermo Scientific GENESYS 180 UV–visible spectrophotometer.

2.6 Fabrication of Biomass–PVA/ZnO Biocomposite Films

PVA (1 g) was dissolved in 50 mL of deionized water at 90 °C using an IKA RCT Basic hotplate stirrer. Purified biomass (0.25 g) and glycerol (2 mL) were introduced, followed by continuous mixing for 60 min to obtain a uniform suspension. Glycerol was used as a plasticizer to improve film flexibility and processability. Its volume was maintained constant at 2 mL in every formulation to ensure that the observed property changes were primarily associated with ZnO loading. ZnO nanoparticles were separately incorporated at 1, 3, and 5 wt.%, and each formulation was dispersed in an Elma Elmasonic S 30 H ultrasonic bath. Entrapped air was removed through vacuum filtration using a Sartorius Combisart system. The entire film-forming mixture, prepared using 50 mL of deionized water and 2 mL of glycerol, was poured into the casting mold and maintained under ambient conditions until complete film formation. A consistent formulation volume and identical drying conditions were maintained for all films to control thickness variation. ZnO loading was calculated relative to the combined dry mass of PVA and purified biomass (1.25 g), excluding water and glycerol.

Table 1. Composition of biomass–PVA/ZnO film formulations

Formulation	PVA (g)	Purified Biomass (g)	Glycerol (mL)	Water (mL)	ZnO Loading (wt.%)	ZnO Mass (mg)
Biomass–PVA	1	0.25	2	50	0	0
Biomass–PVA–1 wt.% ZnO	1	0.25	2	50	1	12.5
Biomass–PVA–3 wt.% ZnO	1	0.25	2	50	3	37.5
Biomass–PVA–5 wt.% ZnO	1	0.25	2	50	5	62.5

2.7 Physicochemical and Mechanical Evaluation

Film thickness was recorded at five locations using a Mitutoyo 293-240 digital micrometer with 0.001

mm resolution, and measurements were expressed as mean ± standard deviation. Structural, chemical, morphological, and elemental features were examined using PANalytical Empyrean XRD, Shimadzu IRSpirit FTIR, and SEM–EDX instruments. Thermal transitions were evaluated through two heating cycles from 25 to 300 °C at 10 °C min^{-1} using a DSC 250. Mass reduction was separately quantified with a TA Instruments TGA 550. Mechanical resistance was measured on 50 × 20 mm film strips using an Instron 3345 universal testing system.

2.8 Tensile Performance Assessment

Maximum tensile stress and fracture elongation were evaluated following ASTM D882 using an Instron 3345 universal testing system fitted with a 500 N load cell. Film strips measuring 20 × 8 mm were conditioned at 23 ± 2 °C and 50 ± 5% relative humidity for 48 h before testing. The initial grip separation was 10 mm, and the crosshead speed was maintained at 10 mm min^{-1}. Every specimen was visually screened prior to testing, and samples containing trapped air, perforations, edge damage, or visible cracks were excluded (Li *et al.* 2022). No specimen was excluded solely because of thickness variation. The thickness of each specimen was measured individually and used to calculate tensile stress. Only specimens with visible preparation defects were excluded according to predefined quality-control criteria applied before testing. Five acceptable specimens from each formulation were examined, and the recorded mechanical properties were reported as mean values.

2.9 Swelling Index

The swelling behavior of the composite films was evaluated using pre-dried specimens measuring 20 × 20 mm. The initial dry mass of each specimen (W_0) was recorded using a Mettler Toledo ME204 analytical balance. Each specimen was immersed individually in 20 mL of phosphate-buffered saline at pH 7.4 and maintained at 37 °C in a Memmert IN55 incubator. The specimens were removed after 0.5, 1, 2, 3, and 4 h, gently blotted with filter paper to remove surface liquid, and weighed immediately (W_t). At predetermined intervals, each film was removed, gently blotted with filter paper, and weighed using a Mettler Toledo ME204 balance. Swelling was determined using Eq. (1) (Koshy *et al.* 2026):.

$$SI(\%) = \frac{Wt - Wo}{Wo} \times 100 \quad \ldots (1)$$

2.10 Biodegradation

Environmental breakdown of the composite films was examined through a soil-burial procedure. Specimens were trimmed into 1.5 × 1.5 cm squares, dried, and weighed as W_1 using a Sartorius Entris II BCE224I balance. Each piece was buried separately in a 100 mL vessel containing commercial potting soil maintained at pH 5.0–6.5. An equal initial soil mass was used in all vessels, and 5 mL of deionized water was added daily under identical conditions to minimize moisture variation. However, soil moisture was not measured gravimetrically; therefore, the fixed-volume water addition represents a methodological limitation of this study. Samples were retrieved every two days, carefully cleaned, dried to constant mass in a Binder ED 23 oven, and reweighed as W_2 (Kumar *et al.* 2024).

$$\text{Biodegradation } (\%) = \frac{W_1 - W_2}{W_1} \times 100 \quad \ldots (2)$$

2.11 Antibacterial Activity

Antimicrobial performance was examined against *Escherichia coli* ATCC 8739 and *Staphylococcus aureus* ATCC 29213 (Alnehia *et al.* 2024). Composite films were cut into 10 × 10 mm pieces, and each surface was exposed to ultraviolet radiation for 10 min inside an Esco UV sterilization cabinet. Following 1 day activation in nutrient broth, microbial turbidity was adjusted to 0.5 McFarland with a Grant-bio DEN-1 densitometer and diluted to approximately 1.0×10^5 CFU mL^{-1}. Individual film pieces were transferred into 20 mL of inoculated broth and maintained at 37 °C for 24 h under mild agitation in an Eppendorf Innova 44 incubator shaker. Afterwards, serially diluted cultures were spread onto nutrient agar, incubated, and quantified using a Stuart SC6 Plus colony counter. Three independent tests were completed for every formulation. Inhibition was determined from Eq. (3).

$$A = \frac{B - S}{B} \times 100 \quad \ldots (3)$$

where N_c and N_s denote viable counts for the untreated control and film-treated culture, respectively.

3. RESULTS AND DISCUSSION

3.1 Structural and Functional Analysis of Purified Algal Biomass

Figure 1(a) presents the XRD profile of purified *Cladophora glomerata* biomass recorded with a PANalytical Empyrean diffractometer. A broad reflection near 26° indicates partially ordered polysaccharide-rich domains surrounded by a predominantly non-crystalline biological matrix. This broadened feature confirms the heterogeneous organization of the recovered algal fraction. Figure 1(b) shows its FTIR spectrum acquired using a Shimadzu IRSpirit spectrometer, revealing characteristic surface functional groups.

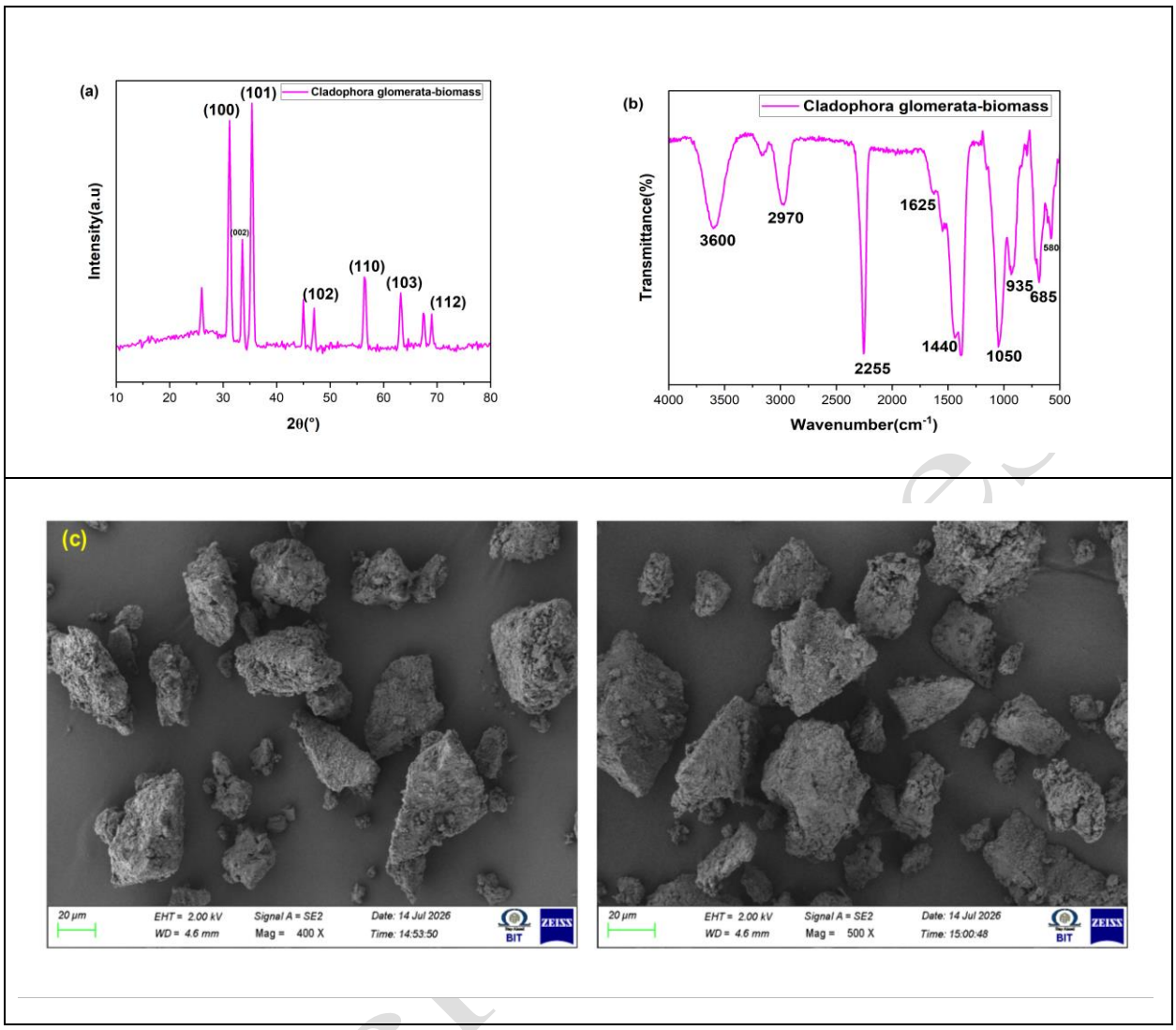

Fig. 1: (a) XRD profile, (b) FTIR and (c) SEM micrographs of purified biomass recovered from *Cladophora glomerata*

The FTIR spectrum showed bands near 2970 and 1440 cm^{-1}, assigned to aliphatic C–H stretching and CH_2 deformation, respectively. The 935 cm^{-1} band was cautiously associated with carbohydrate-related C–O–C or glycosidic vibrations without specifically confirming β-(1→4) linkages. The 1625 cm^{-1} band may contain overlapping contributions from absorbed-water bending and carbonyl-containing groups, while the 1050 cm^{-1} band was assigned to C–O and C–O–C vibrations. Surface examination using a SEM at 20 µm scales revealed an irregular, porous network containing locally compact regions. This heterogeneous architecture provided extensive exposed surface area and numerous sites suitable for interaction with PVA and ZnO nanoparticles.

3.2 Structural Evaluation of Composite Films

Figure 2(a) presents the ordered and disordered phases of biomass–PVA films containing 0, 1, 3, and 5% ZnO, recorded using a PANalytical Empyrean diffractometer.

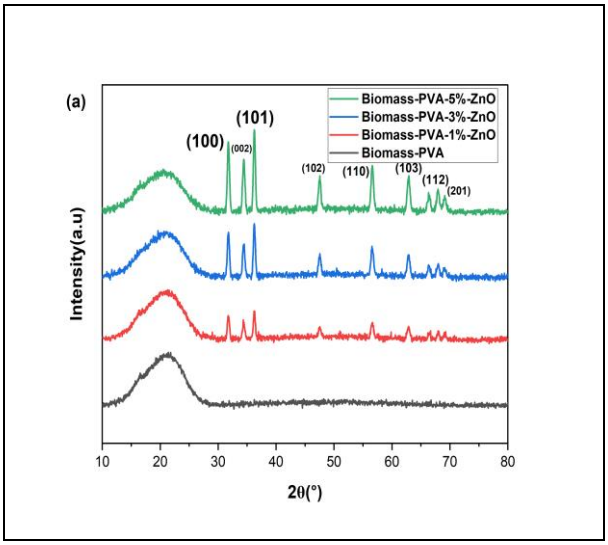

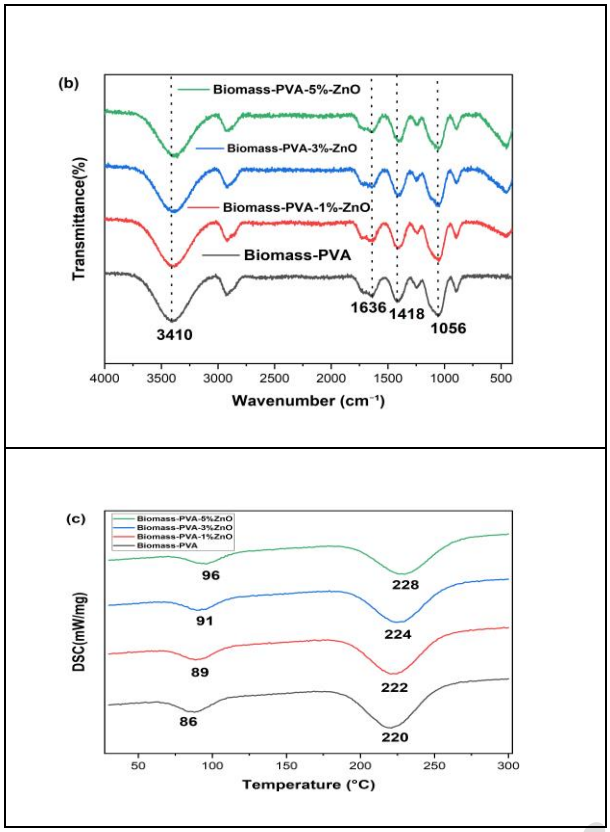

Fig. 2: (a) XRD profiles, (b) FTIR, and (c) DSC thermograms of biomass–PVA films containing different ZnO concentrations

The NETZSCH DSC 214 Polyma thermograms in Fig. 2(c) exhibited a broad endothermic transition at approximately 220–228 °C. This event was assigned primarily to melting and disruption of the semicrystalline PVA-rich domains rather than moisture release, which generally occurs at lower temperatures. The unfilled biomass–PVA film showed a broad transition near 222 °C, while ZnO-containing films exhibited changes in peak position and shape within 220–228 °C. These variations suggest that ZnO incorporation altered polymer-chain organization and interfacial interactions within the matrix. However, DSC alone does not conclusively demonstrate improved thermal stability; therefore, the observed changes are interpreted as modifications in thermal-transition behaviour. The low-temperature transition increased from 86 °C for biomass–PVA to 89, 91, and 96 °C for films containing 1, 3, and 5 wt.% ZnO, respectively. The melting peak similarly shifted from 220 to 222, 224, and 228 °C. The low-temperature event may include overlapping moisture-related effects and was therefore not definitively assigned as T_g.

The PANalytical Empyrean XRD profile of purified biomass displayed a wide reflection near 21.4°, indicating predominantly disordered carbonaceous and polysaccharide-rich regions. After blending with PVA, a broad signal appeared around 19.6°, corresponding to the semicrystalline arrangement of the polymer chains. Increasing ZnO loading increased the intensity of the characteristic ZnO reflections because of the greater crystalline ZnO content in the films. Incorporating increasing quantities of ZnO produced progressively stronger and sharper reflections, confirming successful particle loading (Kumar *et al.* 2025). Figure 3 exhibited characteristic peaks at approximately 31.8°, 34.4°, 36.2°, 47.5°, 56.6°, 62.9°, 67.9°, and 69.1°, indexed to (100), (002), (101), (102), (110), (103), (112), and (201) planes of the hexagonal wurtzite phase, respectively. Figure 3(a) showed mainly near- agglomerated ZnO particle clusters with variable morphology, while the accompanying EDX spectrum confirmed zinc and oxygen as the principal elements. The Thermo Scientific GENESYS 180 spectrum presented in Fig. 4 showed a dominant absorption edge near 339-341 nm, reflecting the optical response of ZnO. Measurements obtained with a Malvern Zetasizer Pro, presented in Fig. 4, yielded a surface potential of approximately -29.29 mV, indicating moderate electrostatic stabilization. However, colloidal stability could not be confirmed without PDI and replicate DLS measurements. The measured hydrodynamic diameter was nearly 340 nm; this comparatively large value resulted from particle clustering in suspension rather than the size of individual crystallites.

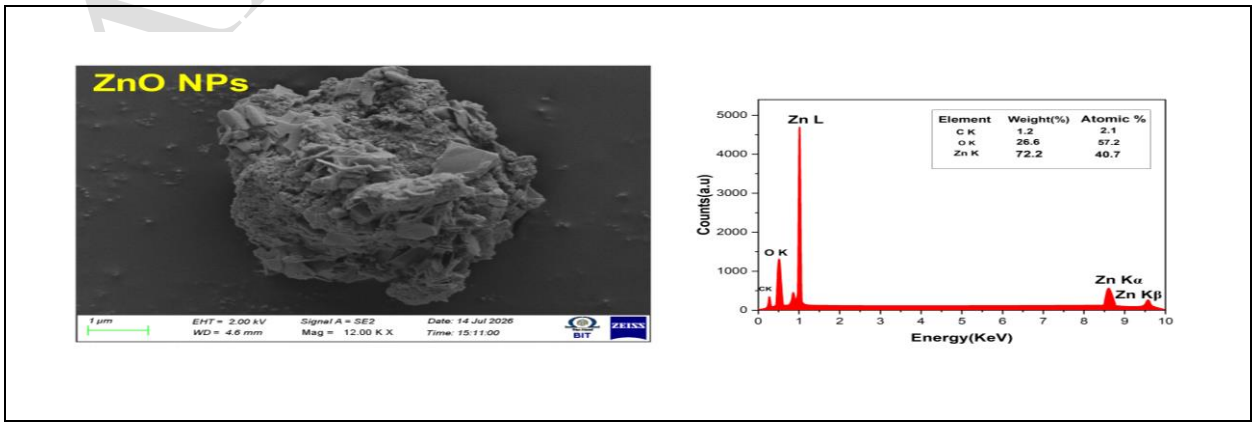

Fig. 3: SEM photos and EDX profile of ZnO NPs

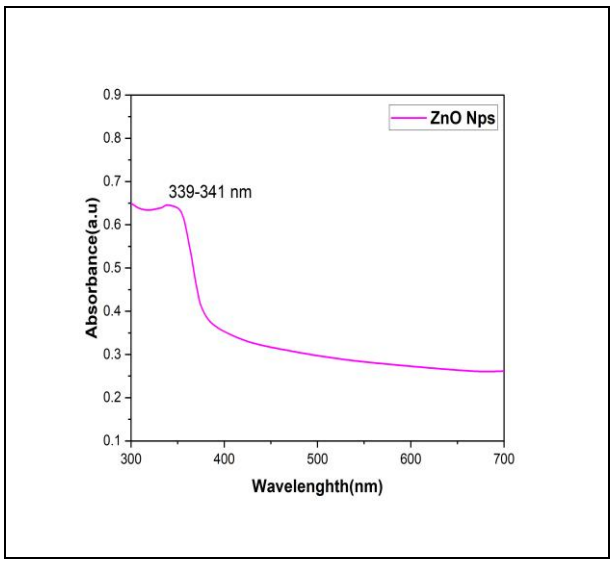

Fig. 4: UV-vis spectrum of ZnO NPs

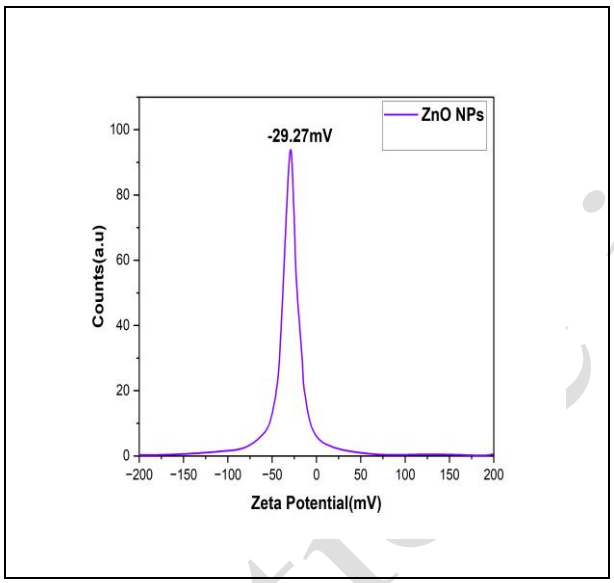

Fig. 5: Zeta potential of ZnO NPs

FTIR profiles of biomass–PVA films containing 0, 1, 3, and 5% ZnO (Figure 6). Spectra collected using a Shimadzu IRSpirit instrument showed a wide absorption region between 3300 and 3500 cm^{-1}, assigned to O–H stretching and hydrogen bonding among the biomass constituents, PVA chains, and nanoparticle surfaces. Signals appearing from 1636 cm^{-1} were associated mainly with carbonyl-containing groups and absorbed water, while changes within this interval suggested intermolecular association rather than definitive formation of new ester linkages. Bands near 1056 cm^{-1} originated from C–O–C and C–O vibrations of carbohydrate-rich components remaining in the purified biomass. A low-wavenumber feature around 500- 600 cm^{-1} was attributed to Zn–O lattice vibration and became more pronounced as the nanoparticle concentration increased. The absorption near 1636 cm^{-1} represented C=O stretching from residual carbonyl groups. The spectrum in Fig. 6 exhibited Zn–O vibrations throughout the 500–600 cm^{-1} region, supporting successful ZnO formation. The observed changes in the O–H, C–O, and carbonyl-related FTIR bands suggest possible interfacial interactions between ZnO and the biomass–PVA matrix. These changes may involve hydrogen bonding or associations between oxygen-containing groups and ZnO surfaces. With increasing ZnO loading, the O–H maximum shifted slightly between 3410 cm^{-1}, accompanied by band broadening. These spectral variations indicate enhanced hydrogen bonding and interfacial association between ZnO particles and the biomass–PVA network.

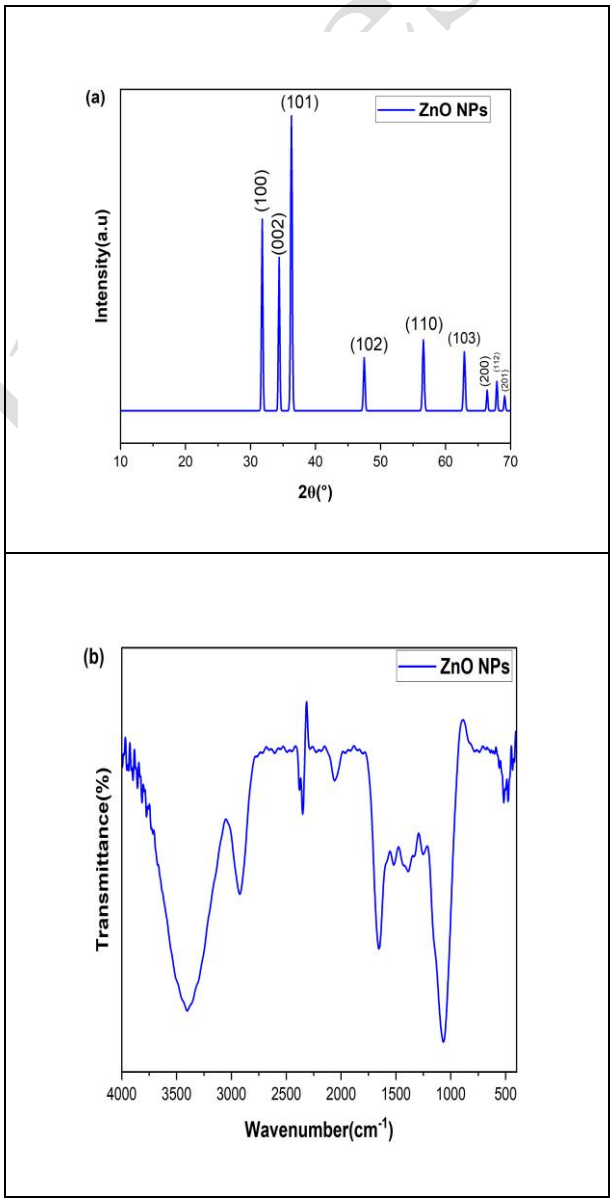

Fig. 6: (a) XRD pattern and (b) FTIR spectrum of ZnO NPs

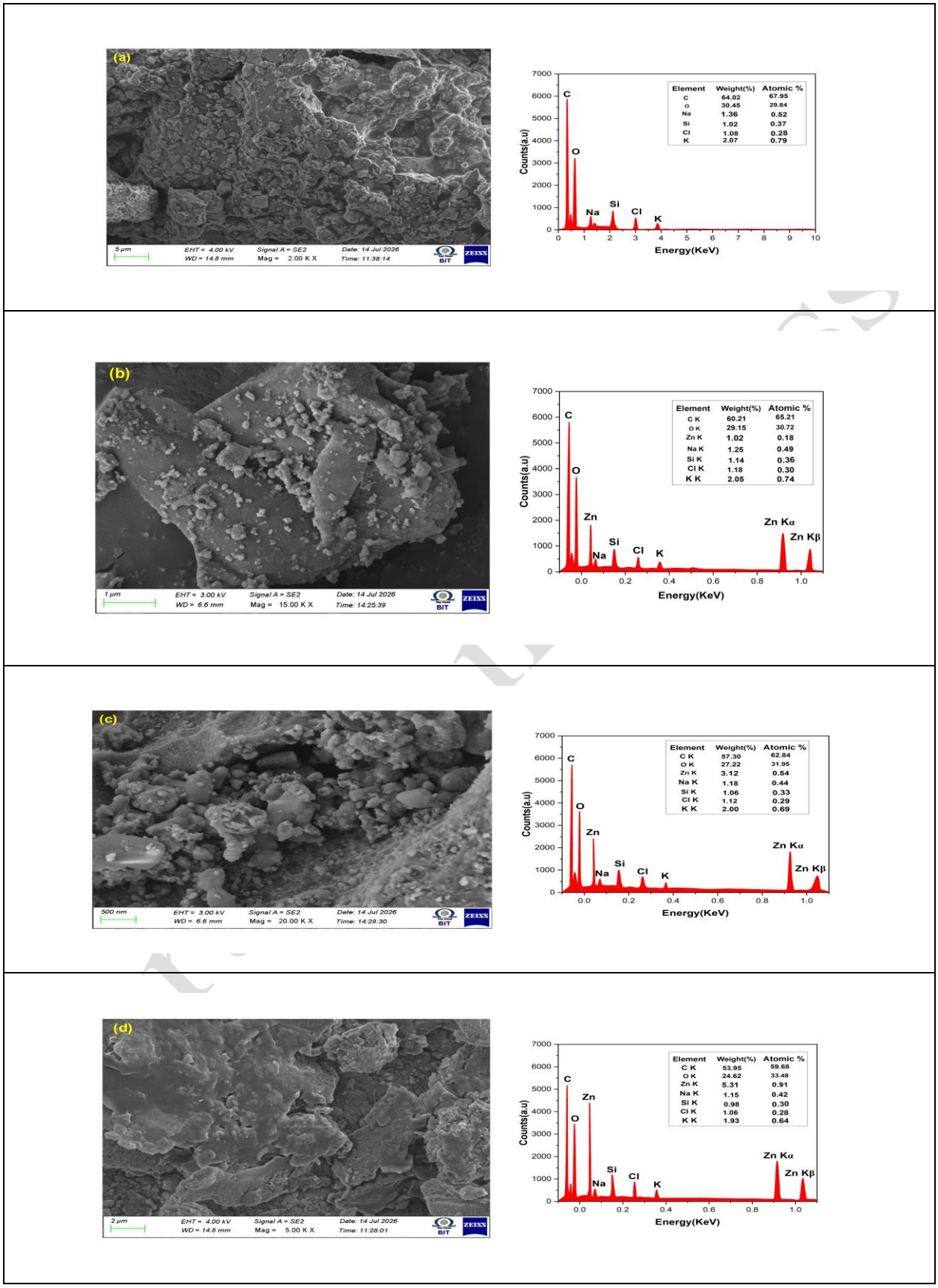

Fig. 7: SEM micrographs and EDX profiles of (a) biomass–PVA, (b) biomass–PVA–1% ZnO, (c) biomass–PVA–3wt % ZnO and (d) biomass–PVA–5% ZnO films

The unfilled matrix displayed a continuous, compact, and comparatively smooth surface, indicating effective blending between PVA and the purified biomass. Introducing ZnO generated small particle clusters and increased surface irregularity. At higher loadings, the films exhibited greater roughness, localized contraction, and a more extensive exposed surface. Although limited agglomeration remained visible, ZnO was distributed throughout the matrix. EDX measurements identified carbon and oxygen in the base film, while zinc signals appeared and progressively intensified in nanoparticle-containing formulations. The accompanying tables provide the measured elemental weight percentages.

3.3 Mechanical Behavior of Composite Films

Film thicknesses were 0.11 ± 0.03, 0.11 ± 0.01, 0.11 ± 0.01, and 0.11 ± 0.01 mm for biomass–PVA, biomass–PVA–1 wt.% ZnO, biomass–PVA–3 wt.% ZnO, and biomass–PVA–5 wt.% ZnO films, respectively. Tensile behaviour was evaluated using an Instron 3345 universal testing system. Maximum stress indicated the force that each film could withstand before it failed, and fracture elongation indicated how much the film could stretch before it failed. As shown in Fig. 8(a), the tensile strength decreased from 11.0 ± 0.3 MPa for the biomass–PVA film to 4.5 ± 0.4, 1.5 ± 0.5, and 2.0 ± 0.5 MPa for films containing 1, 3, and 5 wt.% ZnO, respectively. The elongation at break was 62 ± 4% for biomass–PVA and increased to 90 ± 3% and 85 ± 3% for the 1 and 3 wt.% ZnO films, respectively, before decreasing to 48 ± 3% at 5 wt.% ZnO, as shown in Fig. 8(b). Tensile modulus was not determined in this study. The increasing surface irregularity and particle clusters were observed by SEM. EDX confirmed increasing Zn content with ZnO loading. However, at high loading, particle aggregation probably affected the bond strength between the PVA and the biomass-derived phase. Similarly, in a previous study, A multifunctional bilayer wound dressing comprising a green-synthesized ZnO-reinforced 3D-printed PLA framework and an electrospun PVA–methotrexate nanofibrous layer was developed and exhibited a tensile strength of 34.1 ± 2.1 MPa, Young's modulus of 2100 ± 145 MPa, and a 6-fold improvement in mechanical resilience (Qaeym *et al.* 2026). The localized stress-concentration regions acted as initiation points for cracking and early failure. Therefore, the relatively good dispersion of nanoparticles achieved in the 1% ZnO gave the most favourable flexibility, while a higher amount of ZnO reduced the continuity of the matrix and the mechanical response of the overall material

3.4 Swelling Index

Figure 8(c) illustrates the liquid-uptake profiles of the prepared composite films in phosphate-buffered saline at pH 7.4, measured by a Mettler Toledo ME204 analytical balance.

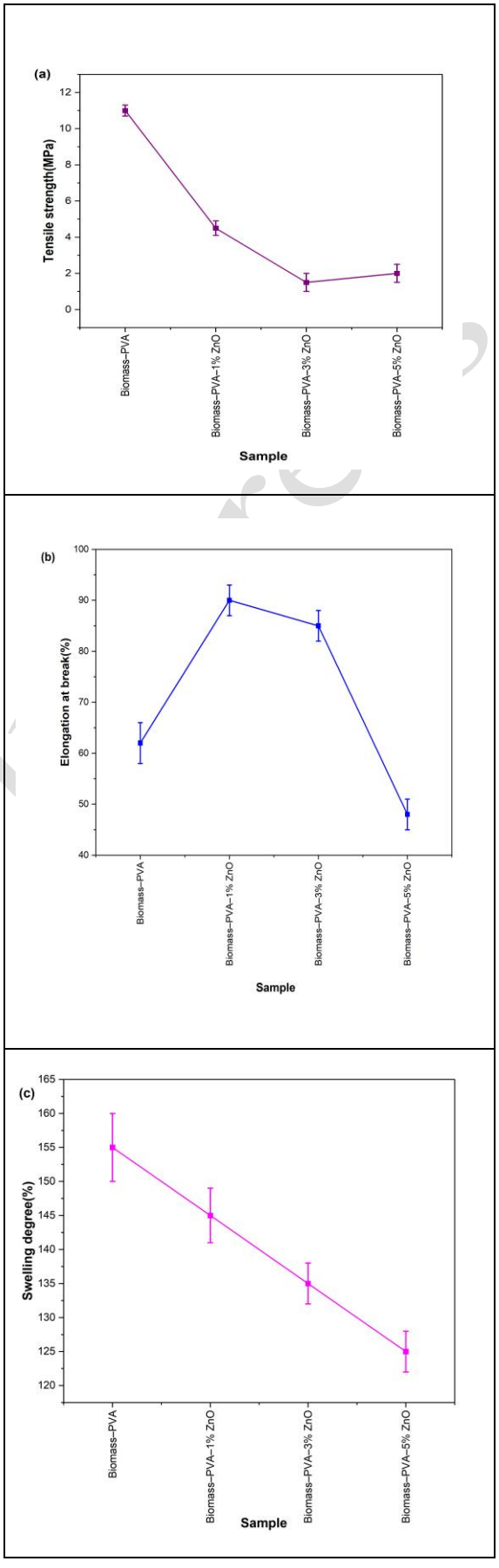

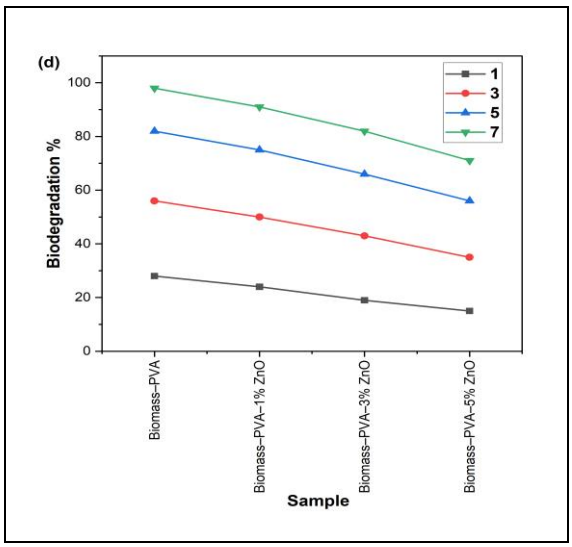

Fig. 8: Properties of biomass–PVA films containing different ZnO levels: (a) maximum tensile stress, (b) fracture elongation, (c) liquid uptake and (d) soil-induced mass loss

The swelling value of the unfilled biomass–PVA film was measured by a Mettler Toledo ME204 balance, and the highest value was obtained, which was 155± 5%. Introducing ZnO significantly lowered liquid absorption, producing values of 145 ± 4%, 135± 3%, and 125 ± 3% for the 1, 3, and 5% formulations, respectively. The reduction was consistent with the denser and irregular surfaces that were seen in the SEM images. The reduction in liquid uptake with increasing ZnO loading may be associated with changes in matrix compactness, particle distribution, and the diffusion pathways available to the liquid. Although ZnO can interact with oxygen-containing groups in the biomass–PVA matrix, it may also introduce polar surface sites. They also reacted with the hydroxyl-rich areas and reduced the number of polar sites available in the structure and capable of hydrogen bonding with water molecules. This resulted in reduced molecular diffusion within the films, due to the increased compactness of the network. The minimum swelling response obtained at 5% ZnO shows the maximum water uptake resistance, which proves that incorporation of nanoparticles decreased the water uptake of the biomass–PVA matrix.

3.5 Biodegradability Studies

The soil-burial behavior was thus observed for 7 days, with samples dried in a Binder ED 23 oven and mass determined on a Sartorius Entris II BCE224I balance. Similarly, biodegradable carboxymethyl cellulose (CMC) films reinforced with pineapple waste-derived green-synthesized ZnO nanoparticles underwent complete soil biodegradation within 9 days, demonstrating improved mechanical, thermal, and environmental performance (Hossain *et al.* 2024).

As presented in Fig. 8(d), Seven-day soil-induced mass loss of biomass–PVA/ZnO films: the unfilled matrix reached 97 ± 1.0%, whereas the formulations containing 1, 3, and 5% ZnO recorded 91 ± 1.0%, 82± 1.0%, and 71 ± 1.0%, respectively ($p<0.05$). The soil-burial mass loss indicates the apparent biodegradation and disintegration behavior of the films under the tested conditions. However, because mineralization was not measured, the results represent a gravimetric assessment of biodegradation rather than definitive evidence of complete chemical biodegradation. These results represent soil-induced mass loss and physical disintegration rather than confirmed chemical biodegradation because dissolution, leaching, and fragmentation were not separately evaluated. All film formulations exhibited more than 70% soil-induced mass loss after seven days, indicating significant disintegration under soil conditions and high disintegration after disposal. The reported values represent percentage mass loss after seven days, not the percentage of material remaining. ZnO incorporation reduced mass loss from 97 ± 1.0% for the ZnO-free film to 91 ± 1.0%, 82 ± 1.0%, and 71 ± 1.0% for films containing 1, 3, and 5 wt.% ZnO, respectively.

3.6 Antibacterial Activity

Figure 9 compares the distinct bacterial inhibition responses of the prepared composite-film formulations, quantified using a Stuart SC6 Plus colony counter.

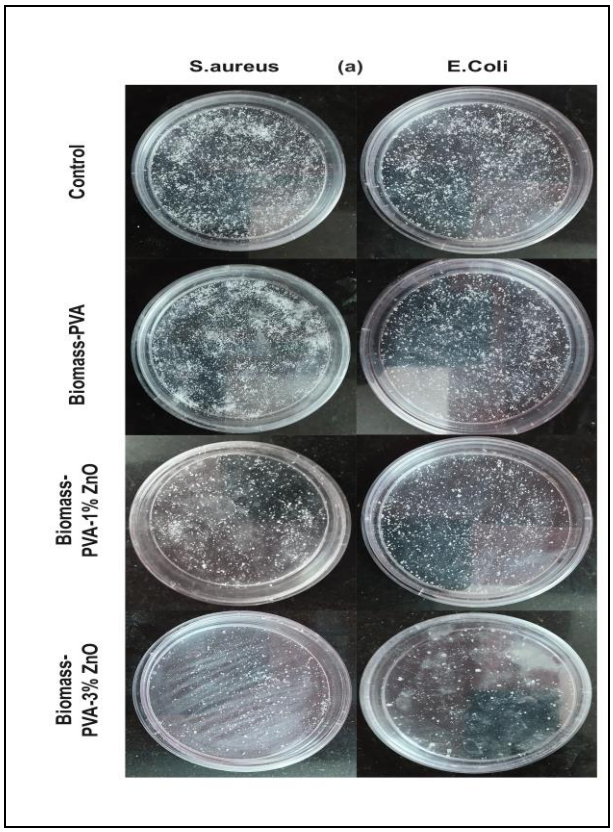

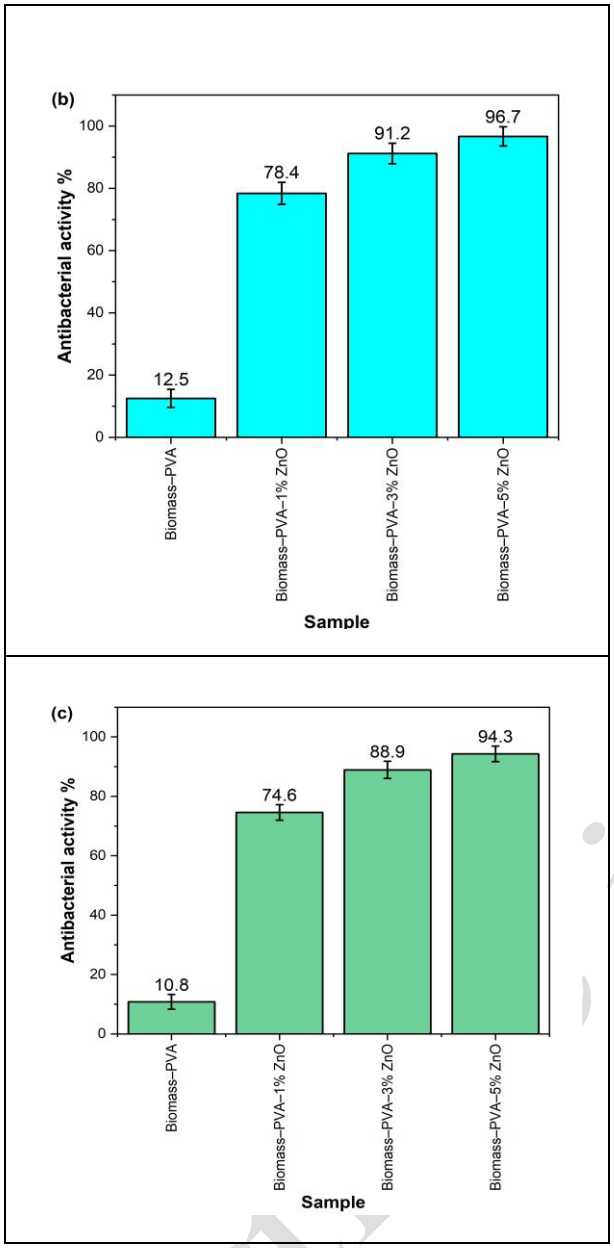

Fig. 9: (a) Antibacterial test images and viable colony results for composite films against (b) *S. aureus* and (c) *E. coli*. Colonies

The ZnO-free biomass–PVA film exhibited antibacterial activities of 12.5±2.9% against *S. aureus* and 10.8±2.5% against *E. coli*. Incorporation of 1, 3, and 5 wt.% ZnO increased the activity to 78.4±3.5%, 91.2±3.3%, and 96.7±3.1% against *S. aureus* and to 74.6±2.6%, 88.9±2.9%, and 94.3±2.6% against *E. coli*, respectively. This comparison demonstrates that ZnO incorporation substantially increased antibacterial performance relative to the ZnO-free film. The biomass–PVA–3wt. % ZnO film achieved antibacterial efficiencies of 88.9 ± 2.9% against *E. coli* and 91.2 ±3.3% against *S. aureus*. Greater sensitivity was consistently observed for *S. aureus*. The antibacterial activity may involve Zn^{2+} release, ROS-mediated oxidative stress, and direct disruption of bacterial membranes. ZnO–polymer interactions may regulate particle exposure and ion release, while aggregation at higher loading could explain the absence of significant improvement between the 3 and 5 wt.% formulations. Likewise, in a previous study, green ZnO nanoparticles were synthesized using Plantago lanceolata leaf extract as a biological medium and produced an antibacterial inhibition zone of 28.11 mm (S. aureus) and 21.21 mm (*E. coli*) (Worku, 2025).

This variation between the Gram-positive and Gram-negative strains can be associated with differences in the thickness, composition, and protective architecture of their cell envelopes.

The effectiveness of the nanoparticles against microorganisms was increasingly observed with the increasing concentration of ZnO in the composite films, which showed that the performance of the composite films was controlled by incorporating the nanoparticles. ZnO has been used globally as an effective broad-spectrum antimicrobial material because it has a number of ways of killing microorganisms. The release of zinc ions from the surface of the particle could disrupt the metabolic processes by reacting with proteins and enzymes in the cell. The direct contact of ZnO particles with the bacterial envelope can also reduce the integrity of the membrane, increase the membrane permeability, and lead to leakage of the contents of the bacterial cell. Besides, ZnO facilitates the generation of excessive ROS that causes oxidative stress and damages membrane lipids, proteins, and genetic material. The joint effect of ionic release, surface interaction, and oxidative damage may eventually inhibit bacterial growth and cause irreversible damage to the cells.

The functional performance of the biomass–PVA films was improved with ZnO incorporation; however, the antibacterial activity did not significantly differ between the 3 and 5% ZnO film formulations ($p>0.05$). The biomass–PVA–3wt.% ZnO film had a swelling value of 135.0%, which was higher than that of the biomass–PVA–5% ZnO film (125.0%), and both of them had similar loss in mass after 7 days in soil. Thus, there was no significant increase in the ability to inhibit the bacteria when the ZnO loading was increased from 3 to 5%, and it was found to decrease its liquid-absorption capacity. The 3wt.% ZnO formulation showed bioefficacy in terms of 3wt.% ZnO showed bioefficacy in the same manner as other formulations but with lower usage and more favorable physicochemical characteristics. Based on the functional performance, resource efficiency, and possible production cost, the biomass–PVA–3 % ZnO composition was found to be optimum. The 3 wt.% ZnO film was preferred for antibacterial performance, with no significant improvement at 5 wt.% ($p > 0.05$). However, the optimal ZnO loading depends on the targeted property.

4. CONCLUSIONS

The environmentally friendly biomass–PVA/ZnO biocomposite film was successfully fabricated using *Cladophora glomerata* as both cellulose-rich reinforcement and a natural reducing/stabilizing agent for green ZnO nanoparticles synthesis. The XRD and FTIR analysis confirmed successful incorporation of ZnO nanoparticles into polymer matrix and the formation of stable composite films while SEM–EDX, UV–Vis, and DSC analysis confirmed the formation of polymer film and stable composite films. The synthesized ZnO nanoparticles exhibited moderate colloidal stability, with an optical absorption edge of 339–341 nm, a zeta potential of −29.29 mV; however, further replicate DLS and PDI measurements are required to establish its colloidal stability. A DLS-derived hydrodynamic diameter of 339–341 nm likely reflects aggregation in suspension rather than the primary nanoparticle size. The use of ZnO resulted in an increase in the thermal transition temperature from 220°C to 228°C, indicating better thermal stability. The tensile strength of the formulations dropped when the ZnO loading was increased, but the 1wt % ZnO formulation still had the highest flexibility, with an elongation at break of 90 ± 3%. The water uptake was significantly reduced from 155 ± 5% (control film) to 125 ± 3% (5 wt.% ZnO composite), showing better resistance to moisture. All films maintained high biodegradability, whereas after 7 days, the loss of soil mass ranged between 71 ± 1% and 97 ± 1% even in the presence of ZnO. The 3 wt.% ZnO composite formulation showed excellent antibacterial activity against both *Staphylococcus aureus* (91.2 ± 3.3%) and *Escherichia coli* (88.9 ± 2.9%) while maintaining good structural stability. Thus, the formulated biomass–PVA/3 wt.% ZnO biocomposite is considered to be the preferred formulation based specifically on antibacterial activity for use in biodegradable packages, wound dressing, and other eco-friendly biomedical uses.

FUNDING

This research received no specific grant from any funding agency in the public, commercial, or not-for-profit sectors.

CONFLICTS OF INTEREST

The authors declare that there is no conflict of interest.

REFERENCES

Abdo, S. M., Youssef, A. M., El-Liethy, M. A. and Ali, G. H., Preparation of simple biodegradable, nontoxic, and antimicrobial PHB/PU/CuO bionanocomposites for safely use as bioplastic material packaging, *Biomass Convers. Biorefine.,* 14(22), 28673–28683 (2024). https://doi.org/10.1007/s13399-022-03591-x

Abhang, L. B., Subramanian, T., Nagabhooshanam, N., Sharma, K., Rao, P. V, Devi, K. M. and LakshmiLavanya, A., Biosynthesize of ZnO nanoparticle from orange fruit peel biomass and its PVA-based composite packaging material: a greener material for suitable packaging, *Biomass Convers. Biorefine.*, 15(9), 14037–14046 (2025). https://doi.org/10.1007/s13399-024-06050-x

Acharya, D., Satapathy, S., Thathapudi, J. J., Somu, P. and Mishra, G., Biogenic synthesis of silver nanoparticles using marine algae *Cladophora glomerata* and evaluation of apoptotic effects in human colon cancer cells, *Mater. Technol.*, 37(8), 569–580 (2022). https://doi.org/10.1080/10667857.2020.1863597

Alnehia, A., Al-Sharabi, A., Al-Hammadi, A. H., Al-Odayni, A. B., Alramadhan, S. A. and Alodeni, R. M., Phyto-mediated synthesis of silver-doped zinc oxide nanoparticles from Plectranthus barbatus leaf extract: optical, morphological, and antibacterial properties, *Biomass Convers. Biorefine.*, 14(15), 17041–17053 (2024). https://doi.org/10.1007/s13399-023-03907-5

Çelekli, A. and Alkan, E., Effect of lead ions on biochemical behavior of *Cladophora glomerata* in sterilized and non-sterilized media, *Protoplasma*, 261(1), 77–87 (2024). https://doi.org/10.1007/s00709-023-01882-2

Chelu, M., Popa, M., Ozon, E. A., Pandele Cusu, J., Anastasescu, M., Surdu, V. A., Calderon Moreno, J. and Musuc, A. M., High-Content Aloe vera Based Hydrogels: Physicochemical and Pharmaceutical Properties, *Polym.*, 15(5), 1312(2023). https://doi.org/10.3390/polym15051312

Ebenezer, A. J. P., Caroline, A. L., Mayakannan, S., Dhivya, M., Sri, T. S. and Saravanan, V., Optimization of Green-synthesized Graphene Quantum Dots using Machine Learning for Neuroprotective Antioxidant Applications, *J. Environ. Nanotechnol.*, 15(2), 463–478(2026). https://doi.org/10.13074/jent.2026.06.2622142

Hossain, M. S., Mohd Azhar, N. I. H. B., Mohd Azman, N. A. B. and Shariffuddin, J. H. Sustainable Food Packaging: Biodegradable Carboxymethyl Cellulose Films Reinforced with Green-Synthesized ZnO Nanoparticles from Pineapple Waste, *Chem. Select*,

9(46), e202404773(2024). https://doi.org/10.1002/slct.202404773

Husien, S., El-azab, W. I. M., Ali, H. R., El-Gendy, N. S. and Mamdouh, W., Valorization of Ulva fasciata biowaste incorporated in PVA nanofibers and films membranes: Box-Behnken optimization toward advanced wastewater treatment and blue economy applications, *Appl. Water Sci.*, 16(4), 132(2026). https://doi.org/10.1007/s13201-026-02807-z

Huynh, T. H. Q., Vu, T. T., Huynh, B. K., Ho, T. G.-T., Do, B. L., Nguyen, T. and Truong, T. B. T., From shrimp shells and banana peels to double-action biopackaging films fighting bacteria and ultraviolet radiation, *Surf. Interf.*, 90, 109212(2026). https://doi.org/10.1016/j.surfin.2026.109212

Jachak, S. R., Srinivasan, R., Arunkumar, S., Kumar, V. N., Manu, Y. M. and Mayakannan, S., Development of MUF-bonded Banyan Fiber Laminates Reinforced with Bio-synthesized CeO_2 Nanoparticles for Advanced Applications, *J. Environ. Nanotechnol.*, 15(2), 554–562 (2026). https://doi.org/10.13074/jent.2026.06.2622149

Kashyap, D. N., Shalom, N., Mayakannan, S., Muthuraj, M., Thanikasalam, A. and Ahmed, A. A., Comparative Green and Wet-chemical Synthesis of ZnO Nanoparticles: Enhanced Photocatalytic and SERS Performance of Defect-rich Nanostructures, *J. Environ. Nanotechnol.*, 15(2), 162–175(2026). https://doi.org/10.13074/jent.2026.06.2612090

Koshy, J. T., Kalumkumvathukkal Sajeev, S., John, A. S. and Sangeetha, D., Development of a pH-Responsive Nanoantibiotic Hydrogel System Based on PVA/Pectin and Biomass-Derived Bacterial Nanocellulose for Antibacterial Wound Dressings, *ACS Appl. Bio Mater.*, 9(3), 1425–1449 (2026). https://doi.org/10.1021/acsabm.5c01934

Kumar, P., Gautam, S., Bansal, D. and Kaur, R., Starch-based antibacterial food packaging with ZnO nanoparticle, *J. Food Sci. Technol.*, 61(1), 178–191 (2024). https://doi.org/10.1007/s13197-023-05834-9

Kumar, V., Singh, Y., Kaushal, S. and Kumar, R., Bioinspired synthesis of copper oxide nanoparticles using aqueous extracts of *Cladophora glomerata* (L.) Kuetz and their potential biomedical applications, *Bioprocess Biosyst. Eng.*, 48(4), 633–646 (2025). https://doi.org/10.1007/s00449-025-03133-5

Li, H., Liu, H., Chen, R., Zheng, S., Xu, Y., Lei, M., Mai, H., Wang, H., Cao, T., Li, L., Zhang, Y., Wang, J. and Cheng, H., Electrospun dressing promotes diabetic-infected wound healing via rapid and sustained antibacterial, ROS scavenging, and immune modulation ability, *J. Nanobiotechnol.*, 24(1), 248(2026). https://doi.org/10.1186/s12951-026-04134-6

Li, J., Zhang, G. and Zhang, D., Structural Optimization of Sorghum Straw Powder/ZnO/PVA Nanocomposite Films, *Coat.*, 12(8), 1226(2022). https://doi.org/10.3390/coatings12081226

Marei, N. H., Abdellatif, A., Saad, G. R., Alkhalifah, D. H. M., Salaheldin, T. A. and Abd El-Samie, E. M., Comparative Study on Boosting Antimicrobial Effectiveness of Chitosan-based Nanoparticles and Films Infused with Royal Jelly, Grape Seed Extract, and Garlic Extract, *Egypt. J. Bot.*, 66(1), 173–188 (2026). https://doi.org/10.21608/ejbo.2025.377114.3272

Mathew, D., Thomas, B., NM, S. and Thomas, J. B., Carboxymethyl Cellulose/Polyvinyl Alcohol/Zinc Oxide Nanocomposite Hydrogel Films for Advanced Wound Dressings, *BioNanoSci,*, 16(4), 272(2026). https://doi.org/10.1007/s12668-026-02508-6

Meera, K. and Ramesan, M. T., Performance of Boehmite Nanoparticles Reinforced Carboxymethyl Chitosan/Polyvinyl Alcohol Blend Nanocomposites Tailored Through Green Synthesis, *J. Polym. Environ.*, 31(2), 447–460 (2023). https://doi.org/10.1007/s10924-022-02649-1

Meniche, A., Fatmi, S., Chibani, N., Ihamouchen, C. and Skiba, M., Valorization of tomato processing waste for the green synthesis of silver nanoparticles and evaluation of their effects on the properties of sodium alginate matrices, *Polym. Bull.*, 83(6), 317(2026). https://doi.org/10.1007/s00289-026-06373-x

Muralidhar, I. K. N., Karagadi, V. A., Naik, M. N. M., Giridhar, M., Jayappa, Y. H., Naik, H. S. N. B., Swamy, B. E. K. and Gowdru, M. K., Fabrication, Characterization, and Antibacterial Performance of Polyvinyl Alcohol (PVA)-Zinc Oxide (ZnO) Thin Films for Packaging Applications, *Appl. Biochem. Biotechnol.*, 198(2), 1165–1180(2026). https://doi.org/10.1007/s12010-025-05502-y

Qaeym, A. S., Guven, A., Ekmen, M., Bingol, A. B., Oktay, B., Ciftci, F. and Ustundag, C. B., Bilayer Wound Dressing Based on Green-Synthesized ZnO-Reinforced 3D-Bioprinted Scaffolds and Electrospun PVA-Methotrexate Nanofibers, *Macromol. Mater. Eng.*, 311(7), e70224(2026). https://doi.org/10.1002/mame.70224

Ramesan, M. T., Jayan, S., Kalladi, A. J., Meera, K. and Sunojkumar, P., Green blend nanocomposites developed from waste sericin, polyvinyl alcohol and boehmite for flexible electronic devices, *Ceram. Int.*, 50(19), 36570–36579 (2024). https://doi.org/10.1016/j.ceramint.2024.07.043

Sahu, D. K., Pradhan, D., Halder, J., Biswasroy, P., Kar, B., Ghosh, G. and Rath, G., Preparation and Characterization of Gatifloxacin-Loaded Polyacrylonitrile Nanofiber for the Management of Dry Eye Infection, *J. Pharma. Innov.*, 18(2), 391–403(2023). https://doi.org/10.1007/s12247-022-09650-0

Sahu, S., Kumar, C., Kaur, A., Khatri, M. and Arya, S. K., Engineering algal nanocellulose–reinforced PVA bioplastics for material-enabled seed coating processes, *Waste Manage.*, 218, 115527(2026). https://doi.org/10.1016/j.wasman.2026.115527

Sethulekshmi, A. S., Joseph, K., Santhosh Aprem, A., Sisupal, S. B. and Saritha, A., Green synthesis of multifunctional natural rubber-lignin nanocomposites: A sustainable approach for waste reduction, *Int. J. Bio. Macromol.*, 280, 135887(2024). https://doi.org/10.1016/j.ijbiomac.2024.135887

Sezen, G. and Aktan, R., Green Synthesis of Zinc Oxide Particles Using *Cladophora glomerata* L. (Kütz) Extract: Comparative Study of Crystal Structure, Surface Chemistry, and Antimicrobial Efficacy with Different Zinc Precursors, *Processes*, 13(8), 2350(2025). https://doi.org/10.3390/pr13082350

Singh, R., Sharma, R., Pal, K., Kant, R., Bergey, E. A., Kumar, D. and Pandey, L. K., Carbon dioxide sequestration, bioremediation, and production of value-added products from freshwater filamentous green algae, *Syst. Microbio. Biomanuf.*, 6(2), 41(2026). https://doi.org/10.1007/s43393-026-00438-8

Venkatesan, R., Sivaprakash, P., Kim, I., Tawfeek, A. M. and Kim, S. C., Green synthesis of carbon nanoparticle-reinforced nanocomposites with gallic acid as a crosslinking agent on poly (butylene adipate-co-terephthalate): Preparation, characterization, and performances, *Indus. Crops and Products*, *209*. (2024). https://doi.org/10.1016/j.indcrop.2023.117949

Worku, L. A., In Vitro Photocatalytic, Antioxidant, and Antibacterial Activity of Biogenically Synthesized Zinc Oxide Nanoparticles via Plantago lanceolata Leaf Extract, *Nat. Prod. Commun.*, 20(12), 404203(2025). https://doi.org/10.1177/1934578X251404203

Xie, Y., Cai, P., Cao, X., Bo, C. and Pan, Y., Water-Resistant Poly(vinyl alcohol)/ZnO Nanopillar Composite Films for Antibacterial Packaging, *ACS Omega*, 9(51), 50403-50413(2024). https://doi.org/10.1021/acsomega.4c07173

Yao, L., Sun, H., Yu, C. and Weng, Y., Enhanced Xylan/PVA Composite Films *via* Nano-ZnO Reinforcement for Sustainable Food Packaging, *Polym.*, 17(8), 1080(2025). https://doi.org/10.3390/polym17081080

Zhang, G., Zhang, D., Li, J., Wang, H., Jin, L., Yi, R., Zhang, Z. and Zhang, Y., Effect of Different Film-forming Temperature on Physicochemical Properties and Microstructure of Sorghum Straw Powder/NanoZnO/Polyvinyl Alcohol Nanocomposite Film, *Sci. Technol. Food Indus.*, 44(9), 127–134 (2023). https://doi.org/10.13386/j.issn1002-0306.2022070290